Inorganica Chimica Acta 471 (2018) 440–445

Contents lists available at ScienceDirect

Inorganica Chimica Acta

journal homepage: www.elsevier.com/locate/ica

Research paper

Facile synthesis of nano-sized MIL-101(Cr) with the addition of acetic acid

Tian Zhao [a,1,*], Ling Yang [a,1], Peiyong Feng [a], Irina Gruber [b], Christoph Janiak [b], Yuejun Liu [a,*]

[a] Key Laboratory of Advanced Packaging Materials and Technology of Hunan Province, School of Packaging and Materials Engineering, Hunan University of Technology, Zhuzhou 412007, China
[b] Institut für Anorganische Chemie und Strukturchemie, Universität Düsseldorf, Universitätsstr. 1, D-40225 Düsseldorf, Germany

ARTICLE INFO

Article history:
Received 13 September 2017
Received in revised form 16 November 2017
Accepted 17 November 2017
Available online 21 November 2017

Keywords:
MOFs
Nano MIL-101(Cr)
Acetic acid
Gram-scale

ABSTRACT

MIL-101(Cr), one of the best investigated and widely used metal–organic frameworks, has been easily synthesized with particle diameters in the range from 387(28) nm to 90(10) nm by using acetic acid as a modulator. The particle size of MIL-101(Cr) decreased with increasing acetic acid concentration. The decrease of size in high concentration of acetic acid may be explained with the efficient suppression of the framework extension. In a selected condition, MIL-101(Cr) possessing an average diameter of about 90 nm can be prepared easily and reproducibly in gram-scale, with high BET-surface areas (3200–3500 m^2/g) and fairly good yield (60–75%).

1. Introduction

Metal-organic frameworks (MOFs) receive great attention [1,2] due to their intriguing structural properties such as high porosity, which led to many potential applications including gas storage [3,4], separations [5,6], catalysis [7,8] and heat transformation [9] etc. Nano-crystalline MOFs (NMOFs) combine the bulk phase properties of the MOF together with the additional physical/chemical properties derived from nano-sized particles, which can display improved properties [10]. Recently, nano-scaled Tb/Eu-MOFs were used as self-calibrating fluorescence sensor for rapid detection of an anthrax biomarker has been reported [11]. Due to their nano-size property, NMOFs have been confirmed more efficient for drug delivery via clathrin-mediated endocytosis [12]. Nano-sized HKUST-1 presented higher CO_2 adsorption capacity than micro-sized counterparts [13]. Nano-ZIF-11 particles were more easily integrated with high loading (10–25 wt%) in a polymeric continuous phase to produce mixed matrix membranes etc. [14].

MIL-101(Cr) [15] is a three-dimensional chromium terephthalate-based porous material with the empirical formula $[Cr_3(O)X(bdc)_3(H_2O)_2]\cdot nH_2O$ (bdc = benzene-1,4-dicarboxylate, X = OH or F). It possesses the framework of augmented MTN zeolite topology. MIL-101(Cr) has two kinds of meospore cages with free diameters of 29 Å and 34 Å, and pore aperture windows of 12 × 12 Å and 16 × 14.7 Å respectively (Fig. S1 in ESI†). MIL-101(Cr) shows high surface area (BET surface area of 4000 m^2/g) [15] and excellent thermal/chemical stability, which makes the material very promising for practical applications [16–19].

Compared to other MOFs, MIL-101(Cr) possesses smaller particle sizes, but still much larger than nanocrystals. Several specific strategies have been reported to synthesize nano-sized MIL-101(Cr) [20–22]. For instance, Jhung and co-workers reported that the MIL-101(Cr) particle size can be decreased to 50 nm with increasing water concentration and pH value via microwave irradiation [22]. Chang and co-workers using HF as additive could get nano-sized MIL-101(Cr) with diameters around 90 nm [23]. Burrows and co-workers showed that nanoparticles of MIL-101(Cr) can be prepared from 19(4) nm to 84(12) nm diameter, by using different monocarboxylic acids as mediator [21]. Recently, in related work highly crystalline MIL-101(Cr), composed of crystals in the size range of 100–150 nm with multifaceted surface, could be obtained in an optimized molar regime of $CrCl_3\cdot 6H_2O/H_2$ bdc/100HCOOH/550H_2O at 210 °C for 8 h [24]. Luo and co-workers recently demonstrated that MIL-101(Cr) with particle sizes around 100 nm can be synthesized by adding prepared nano-MIL-101(Cr) as crystal nuclei [20]. Wuttke and co-workers produced nano-sized MIL-101(Cr) coated by lipid bilayers as a potential novel hybrid nanocarrier system [25]. Iglesia and co-workers reported mixed matrix membranes (MMMs) based on the polyimide Matrimid®

* Corresponding authors.
E-mail addresses: tian_zhao@hut.edu.cn (T. Zhao), yuejun_liu@hut.edu.cn (Y. Liu).
[1] Tian Zhao and Ling Yang contributed equally to this paper.

https://doi.org/10.1016/j.ica.2017.11.030
0020-1693/

Table 1
The summary of surface areas of reported MIL-101(Cr) in recent years.[a]

Additive	Time (h)	Temperature (°C)	Yield (%)[b]	S_{BET} (m^2/g)	V_{pore} (cm^3/g)	Ref.
HF	8	220	~50	~4100	2.02	[15]
HF	8	220	n.a.[b]	2172	1.07	[29]
HF	8	220	n.a.[b]	3517	2.20	[30]
HF	8	220	n.a.[b]	2231	1.08	[31]
HF	8	220	n.a.[b]	2233	1.20	[32]
HF	8	220	n.a.[b]	2651	1.29	[33]
HF	8	220	n.a.[b]	2846	1.30	[34]
HF	8	220	n.a.[b]	2995	1.31	[35]
HF	8	220	~53	3007	1.51	[36]
HF	8	220	~50	2720	1.45	[37]
HF	8	220	38	2887	1.45	[38]
HF	8	220	n.a.[b]	2618	1.55	[39]
HF	8	220	n.a.[b]	2350	1.22	[40]
HF	8	220	n.a.[b]	3312	1.57	[41]
HF	8	220	n.a.[b]	3302	1.54	[42]
HF	8	220	n.a.[b]	2852	1.32	[43]
HF	8	220	n.a.[b]	~3115	1.58	[44]
TMAOH[c]	24	180	~47	~3055	1.51	[7]
TMAOH[c]	24	180	~50	~3060	1.45	[19,45]

[a] In principle following the original hydrothermal synthesis procedure by Férey et al. [15].
[b] The yield is based on Cr and refers to the isolated material after the washing procedures. When no yields were given (n.a.) and the original procedure by Férey et al. [15] was followed, a yield of ~50% can be assumed. We note that significant water uptake of ~1 g(H_2O)/g(MIL) can occur at 40–50% room humidity which will lead to higher weights than the truly empty material.
[c] TMAOH = tetramethylammonium hydroxide.

with nano-sized MIL-101(Cr) as promising materials for use in membrane reactors for esterification reactions [26].

At the same time, the initial MIL-101(Cr) synthesis reports a fluorine-free route but also the addition of an equimolar amount of hydrofluoric acid (HF) to chromium and H_2bdc, and the obtained products are isostructural [15]. The concomitant drawbacks are the toxicity of hydrofluoric acid, relatively low yield of about 50%, and doubtful reproducibility, as there is a large spread of surface area values, with most of them in the interval of 2200–3500 m^2/g (further details please see Table 1). The work-up procedures are tedious, and include double filtrations for separation of larger crystals of terephthalic acid and prolonged washings, including such environmentally non-benign agents as NH_4F [27]. Recently, we reported an improved MIL-101(Cr) synthesis method with HNO_3, which could increase the yield to over 80% with the BET surface area (>3100 m^2/g) lagging only ~10% behind compared to the use of HF [28]. However, nitric acid is a strong acid, which may pose danger to human health or enhance metal corrosion in autoclaves. Hence here, we propose a facile hydrothermal method to control MIL-101(Cr) particle size from 387(28) nm to 90(10) nm by using acetic acid as a modulator, which has not been reported previously. The nano-sized MIL-101(Cr) with sizes of around 90 nm can be produced with high specific surface areas and moderate to good yield.

2. Results and discussion

By trying to obtain nano-sized MIL-101(Cr), varied amounts of acetic acid were used as additive in the synthesis to reveal the optimal synthetic conditions. During these experiments, we found that acetic acid led to a significant decrease in particle size of MIL-101(Cr) to the nano-scale (average size ~90 nm) with BET surface areas around or over 3200 m^2/g. A remarkable amount of terephthalic acid can still be present inside the pores and mixed with the MIL-101(Cr) crystallites. The residual reactants and eventually the solvent needed to be removed from the pores in order to obtain a product as porous as possible. All synthesis materials underwent the same purification, which is, washing and drying (activation) procedure. The products synthesized in this work avoided using HF, thus, the formula of this work should not contain F atoms and considered as $[Cr_3(O)X(bdc)_3(H_2O)_2]\cdot nH_2O$ with X = OH (n = ~25).

The reaction was carried out with addition of 5, 10, 15, 20, 25, 30, 35 and 40 mL of acetic acid (A). Products were named as A-5, A-10, A-15, A-20, A-25, A-30, A-35 and A-40 respectively. The sample without acetic acid was named A-0. All these experiments were carried out with 30 mmol each of chromium(III) nitrate nonahydrate and 30.1 mmol of terephthalic acid in a PTFE- (Teflon-) lined autoclave at 220 °C for 20 h (see Exp. section). The experiments under the same acetic acid concentration at 220 °C for 8 h were also conducted. However, the yields and porosity of products with 8 h are much lower than that of 20 h reactions (see Table 2 and Table S1 in the ESI†). After hydrothermal reaction, the purification of products followed as described in the experimental section.

In this work, with the increase of concentration of acetic acid, the products became more and more difficult to separate by centrifugation, which indicated that the particle size of products became smaller and smaller. Scanning electron microscopy (SEM) (Fig. 1) showed the acetic acid-dependent evolution of MIL-101 (Cr) particles. The average particle size of acetic acid-modulated MIL-101(Cr) was analysed using a Gaussian model and is given in Table 2. The particle size distribution of sample A-0–A-30 is presented in Fig. S3 in the ESI†. The increase in acetic acid from A-0 to A-30 demonstrated a clear tendency for decrease on average particle size with higher concentration of acetic acid (Fig. 1, Fig. S3 in ESI†). However, the SEM images of A-35 and A-40 showed many rod-like materials with micron-size, which indicated a by-product

Table 2
Yield, particle size, surface area and pore volume for MIL-101(Cr)-20 h with various amounts of acetic acid (A) as additive (BET calculations [46] please see Fig. S2 in the ESI†).

Sample-X with X with X = mL, acetic acid (concentration acet. acid /.mmol/mL)	Molar ratio A:Cr:bdc	Initial pH	Yield (%)[a]	Particle size (nm)[b]	S_{BET} (m^2/g)[c]	$S_{Langmuir}$ (m^2/g)	V_{pore} (cm^3/g)[d]	N_2 uptake (cm^3/g)[d]
A-0 (0)	0:1:1	2.3	62.8	387 (28)	2860	3840	1.49	917
A-5 (0.58)	2.9:1:1	2.2	73.2	383 (25)	3020	4120	1.66	974
A-10 (1.17)	5.8:1:1	2.1	75.6	346 (19)	3070	4490	1.65	980
A-15 (1.75)	8.7:1:1	2.0	70.8	279 (21)	2960	4230	1.66	1063
A-20 (2.33)	11.7:1:1	1.8	71.2	160 (16)	3550	4820	2.38	1385
A-25 (2.91)	14.6:1:1	1.6	68.2	148 (14)	3420	4650	2.32	1351
A-30 (3.50)	17.5:1:1	1.4	65.8	90 (10)	3220	4430	2.12	1270
A-35 (4.08)	20.4:1:1	1.3	41.8	–	1690	2360	1.32	749
A-40 (4.66)	23.3:1:1	1.2	25.0	–	1570	2070	1.30	715

[a] The Cr:bdc ratio is always 1:1, and the yield is based on Cr.
[b] The average particle size was analysed using a Gaussian model and estimated standard deviations are given in parentheses. A-35 and A-40 contained too many rod-like by-products, thus, there was no sense to calculate their average particle sizes.
[c] Calculated in the pressure range $0.05 < p/p_0 < 0.2$ from N_2 sorption isotherm at 77 K with an estimated standard deviation of ±50 m^2/g.
[d] Calculated from N_2 sorption isotherm at 77 K ($p/p_0 = 0.97$) for pores ≤20 nm.

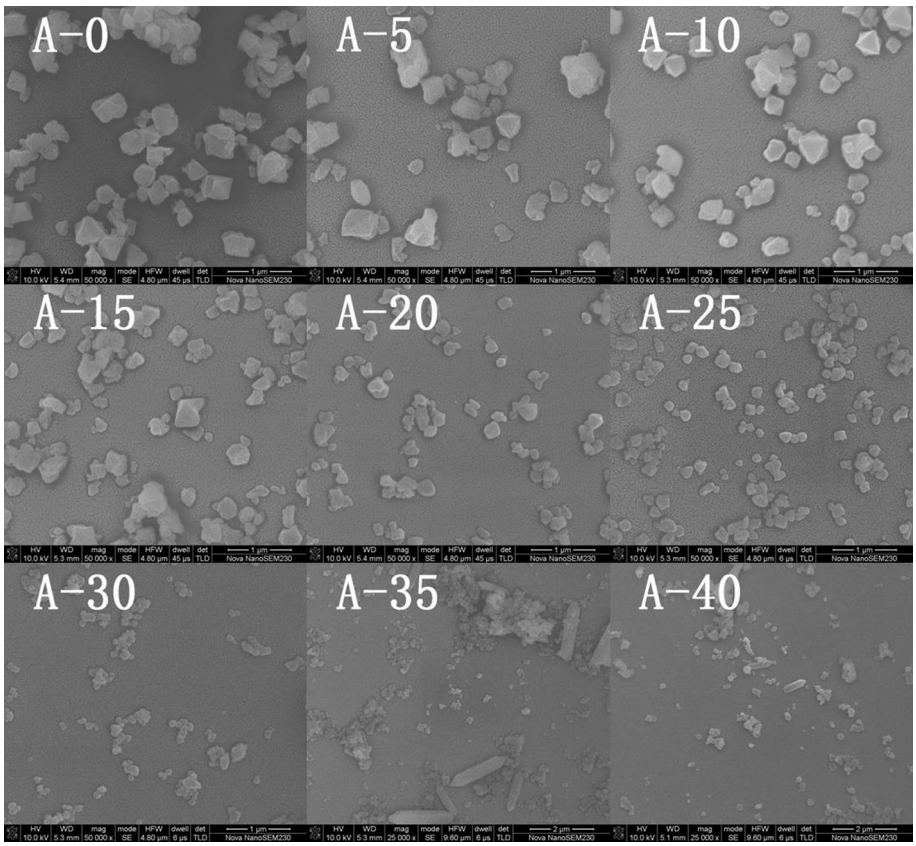

Fig. 1. SEM images of acetic acid-variable MIL-101(Cr) samples. The length of the scale bar is always 1 μm, except for samples A-35 and A-40 where it is 2 μm.

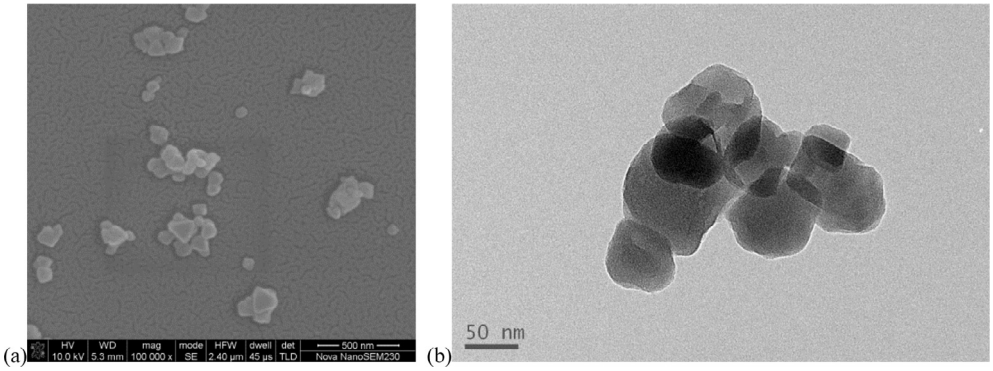

Fig. 2. SEM image and TEM image of A-30, which possessed the smallest particle size of MIL-101(Cr).

had been formed at higher concentration of acetic acid condition. Due to too many rod-like by-products in A-35 and A-40 (Fig. 1), their average particle size increased instead. It is worth to notice that A-30 possessed an average diameter of ~90 nm, which can be deemed as nanomaterials. The smallest MIL-101(Cr) (A-30) was also characterized by transmission electron microscopy (TEM), which was in line with the results of the SEM image (Fig. 2).

A-0, A-5 and A-10 showed relatively large size particles (>340 nm, Table 2), with most of them being of octahedral shape, which is the typical morphology of MIL-101(Cr) [7,9,38,45]. With increasing concentration of acetic acid to 0.58 or 1.17 mmol/mL, the average diameter of MIL-101(Cr) decreased slowly and most particles still kept the octahedral morphology. While the concentration of acetic acid was further increased from 1.17 to 3.5 mmol/mL, the average diameter of MIL-101(Cr) presented an almost linear descent (Fig. S3 in ESI†). The particle size of MIL-101(Cr) was only around 90 nm at a concentration of acetic acid of 3.5 mmol/mL (A-30). At the same time, the SEM images of A-15, A-20, A-25 and A-30 disclosed that the octahedral particles became fewer and irregular shaped particles became more dominant with increasing acetic acid content. Moreover, the particles which are synthesized at lower pH value (1.4 in A-30) are of smaller size, and with a little bit lower yields (Table 2). That is because a low pH may not beneficial to produce benzenedicarboxylate and chromium trimers [22]. In the previously reported literature [21–23,25], researchers preferred a higher pH or diluted reactants

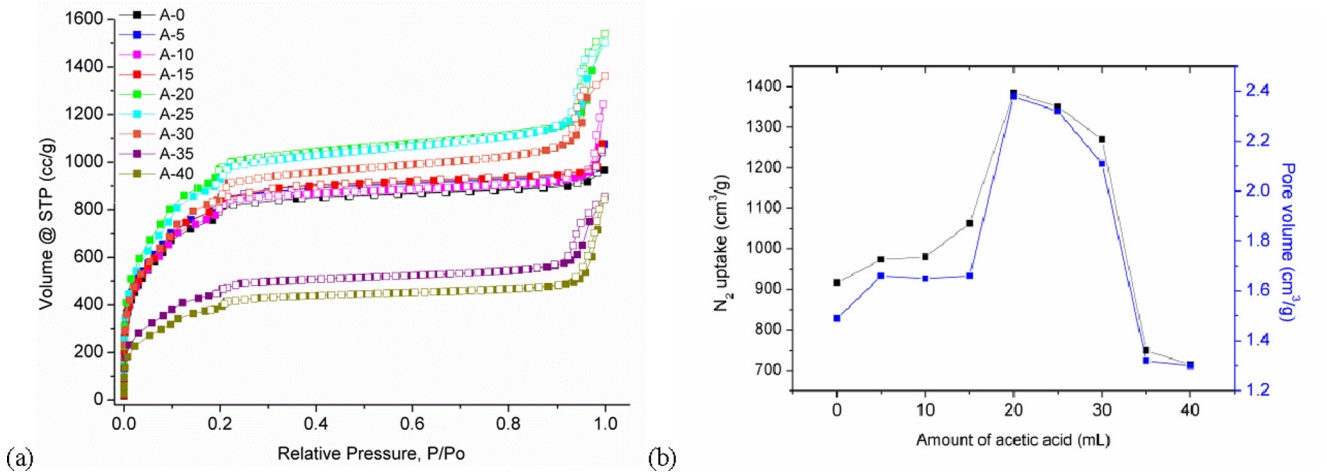

Fig. 3. (a) N_2 adsorption–desorption isotherms of acetic acid-modulated MIL-101(Cr); filled symbols are for adsorption, empty symbols for desorption. (b) Plot of pore volume (at $p/p_0 = 0.97$ for pores $\leq$20 nm) and N_2 uptake (at $p/p_0 = 0.97$) versus amounts of acetic acid.

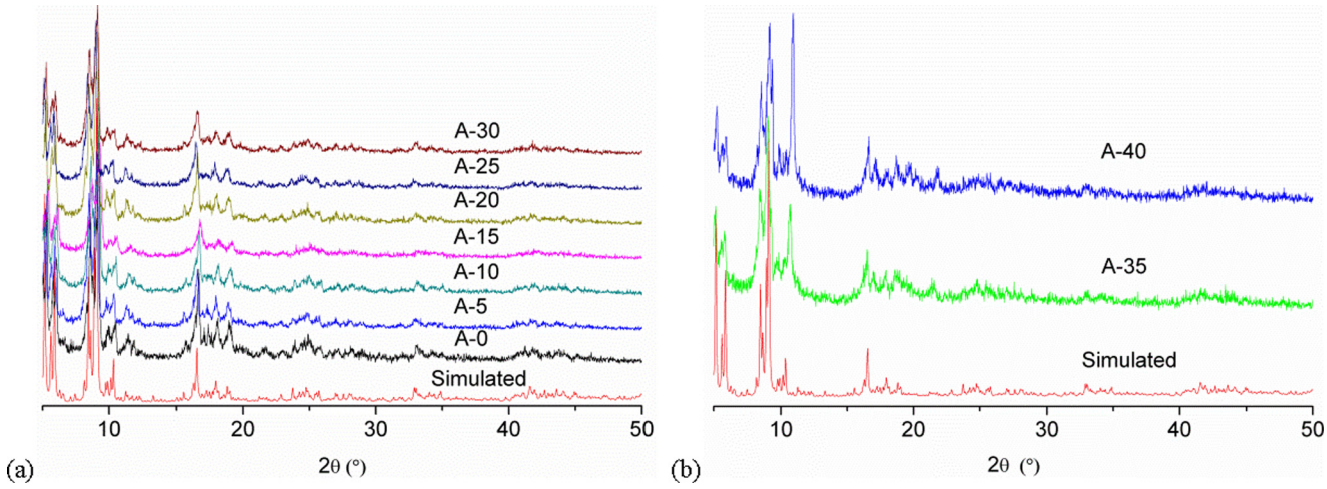

Fig. 4. The PXRD patterns of acetic acid-variable MIL-101(Cr) compared with simulated pattern. (a) Sample A-0–A-30, (b) A-35 and A-40.

conditions to produce nano-sized MIL-101(Cr). But in our work, we proved that, with the presence of acetic acid with lower pH, also could synthesize nano-MIL-101(Cr) successfully.

To confirm that the experiment A-30 can be reproduced, two repeated experiments were conducted. The TEM images and analytical porosity results are presented in Fig. S4 and Table S2 in ESI†, which revealed quite good reproducibility. The purity of A-30 was analyzed by CHN and energy-dispersive X-ray spectrometric (EDX) elemental analysis (for element mapping please see Fig. S5). Before elemental analysis, A-30 was dried in a vacuum oven (120 °C, 12 mbar) for 2 h. Calcd. for $[Cr_3(O)(OH)(bdc)_3(H_2O)_2]\cdot 2H_2O$: C 38.26, H 2.81, N 0, Cr 20.70; found C 38.65, H 2.98, N 0.00. From EDX analysis, the atom ratio C/Cr = 8.4 (calc. 8.0) is in good agreement with the formula. The element mapping results also proved that A-30 possesses very good purity.

The analytical results showed that a good yield and product quality could be reached compared to experiments without addition of acetic acid (Table 1). Concerning the yield it should be noted that in the literature the yields of MIL-101(Cr) materials with a surface area in the range from 2200 to 3500 m^2/g (see Table 1) are relatively low for most syntheses. In particular the HF-based synthesis only gives yields of about 50% (Table 1) [15].

Nitrogen sorption isotherms of acetic acid-modulated MIL-101 (Cr) are shown in Fig. 3a, which are typical type I(b) sorption isotherms [47] as reported in the literature for MIL-101(Cr) [15]. The Brunauer-Emmett-Teller (BET) surface area and porosity results were shown in Table 2. Obviously, A-20 and A-25 possessed the best porosity, with the BET surface area over 3400 m^2/g. A-30, with nano-scale size, also showed very high BET surface area (3220 m^2/g) and total pore volume (2.12 cm^3/g). Nevertheless, with the addition of acetic acid, most products showed very good quality and yield, except A-35 and A-40. It is worth to notice that, when the concentration of acetic acid was over 3.5 mmol/mL, the pore volume and amount of adsorbed nitrogen of the products presented a sharp decline (Fig. 3b). This indicated that, under too high acetic acid concentration condition, there is no positive effect for MIL-101(Cr) synthesis, and the by-product which is MIL-53 showed much lower porosity. Furthermore, high doses of acetic acid (A-45 and A-50) were also tested in MIL-101(Cr) synthesis. In those two experiments, only off-green solids were obtained in quite small amounts, which showed no porosity. Thus, in this work, the limiting amount of acetic acid as additive is 30 mL (corresponding to a molar ratio of acetic acid to Cr of 17.5:1). In previous work, we reported that, in small scale synthesis (5 mL) of MIL-101(Cr), with the addition of acetic acid and 'seeds' we could largely decrease the reaction temperature (from 220 °C to 160 °C) [28]. In that case, the limiting concentration of acetic acid as additive was only half of that in this work. This is because, in this work,

we prolonged the reaction time from 8 h to 20 h, and in the case of large scale synthesis, the synthesis condition can be different from small scale synthesis [28]. However, a comparison experiment with the same concentration of acetic acid as A-30 in small scale synthesis (5 mL) also had been conducted. In this experiment, the reaction time was prolonged from 8 h to 20 h, and some solid product was obtained. It still possesses relatively high BET surface area (2940^2/g), but the yield was only 19%. And the particle size seemed bigger than that of A-30, due to its much easier separation by centrifugation. This probably indicated that, under the same concentrations of reaction reagents, it's more difficult to get nano-sized MIL-101 (Cr) for a small-scale hydrothermal synthesis.

The pore size distribution curve and cumulative pore volume curve for A-30 were analyzed by NL-DFT method (Fig. S6 in ESI†) and are similar to the reported pore size distribution for MIL-101(Cr) [48,49]. The thermogravimetric (TG) curve of A-30 revealed that nano-MIL-101(Cr) also presented high thermal stability as originally reported [15] (Fig. S7 in ESI†).

The powder X-ray diffractograms (PXRD) of the MIL-101(Cr) samples (A-0–A-30) with acetic acid as an additive can all be positively matched to the simulated PXRD pattern which was generated from the deposited X-ray data file at the Cambridge Structure Database (CSD-Refcode OCUNAK) using the program MERCURY (Fig. 4a). While the patterns of A-35 and A-40 possessed a stronger reflection at $2\theta = 10.92°$, which pointed to the rod-like by-product (MIL-53) which had been detected in SEM images (Fig. 4b). This is not surprising since MIL-53 is a more thermodynamically stable product than MIL-101. The presence of MIL-53 is difficult to detect by PXRD since its strong reflexes overlap with those for MIL-101. The comparison of powder X-ray diffractograms of A-35 and A-40 to the simulated PXRD pattern of MIL-53 is presented in Fig. S8 in ESI†. The simulated PXRD pattern of MIL-53 was generated from the deposited X-ray data file at the Cambridge Structure Database (CSD-Refcode QONQEQ and QONOAM) using the program MERCURY.

It has been reported that, for carboxylate-based MOFs, the use of high concentrations of monocarboxylic acid [50,21] or higher pH [22] in the syntheses restricts nucleation and enables to form large crystals. However, in the present case, higher concentrations of acetic acid yielded smaller crystals, because of the efficient suppression of the framework extension [51] of MIL-101(Cr). With the high excess of acetic acid of about 20:1:1 for A:Cr:bdc in the samples where nano-MIL-101 was formed, we propose that the high amount of modulator molecules will cover indeed the growing crystals. At the same time, crystallization will start at many nucleation points, that is, trinuclear chromium complexes, which have formed in solution. Such nucleation points can continue to form even when the crystal growth at previous nucleation points proceeds. With a slow growth rate due to the high excess of modulator the new nucleation points can still add to the crystal growth process. The more nucleation points and crystal seeds there are, the smaller the crystals will remain as eventually all chromium and H_2bdc starting material will have been consumed so that crystal growth comes to an end. If the small crystals are covered and shielded by the modulator then the process of Ostwald ripening, which could have led to larger crystals, may also be slowed down significantly.

3. Conclusions

In summary, we have demonstrated that the particle size of MIL-101(Cr) can be adjusted from 387(28) nm to 90(10) nm by adding acetic acid as modulator. The nano-sized MIL-101(Cr) with average diameter around 90 nm can be obtained under high acetic acid concentration condition of 3.5 mmol/mL (Molar ratio A:Cr:bdc = 17.5:1:1). Nano-MIL-101(Cr) showed high specific BET-surface areas (>3200 m^2/g) and moderate to good yield (>60%), and can be prepared in gram-scale. This provides a new facile method to produce nano-sized MIL-101(Cr), and we hope that this work will inspire further investigations into the fabrication of nano-sized chromium-benzenedicarboxylate MOF crystallites for desired applications.

4. Experimental section

4.1. Materials

Chromium(III) nitrate nonahydrate (AR, 99%, Aladdin), benzene-1,4-dicarboxylic acid (99%, Aladdin), acetic acid (AR, 99.5+%, Sinopharm chemical reagent Co., Ltd), N,N-dimethylformamide (DMF, AR, 99.5+%, Sinopharm chemical reagent Co., Ltd) and ethanol (AR, 99.7+%, Sinopharm chemical reagent Co., Ltd). All chemicals were used as obtained from commercial sources without further purification.

4.2. Instrumentation

X-ray diffraction (XRD) measurements were carried out on samples at ambient temperature by using an Ultima IV instrument with a flat sample holder. Simulated PXRD pattern were calculated from single crystal data with the MERCURY 3.0.1 software suite from CCDC.

Nitrogen physisorption isotherms at were measured at 77 K using a NOVA-4200e instrument within a partial pressure range of 10^{-6}–1.0. Before measurements, the samples were degassed at 120 °C for 2 h. The BET surface areas were calculated from adsorption isotherm data points in the pressure range p/p0 = 0.05–0.2.

Thermogravimetric analysis (TGA) was measured on a TGA/DSC1/1100SF instrument at 10 °C/min heating rate using aluminum sample holders and nitrogen as carrier gas.

Scanning electron microscopy (SEM) characterization was prepared by dropping a 15 μL solution on silicon substrates at room temperature with a Nova NanoSEM230.

Transmission electron microscopy (TEM) was conducted on a JEM-2100F instrument by dropping a 3 μL solution onto a carbon-coated Formvar copper grid (300 mesh) followed by solvent evaporation at room temperature.

Elemental (C, H, N) analysis was done with a Perkin-Elmer Series 2 Elemental Analyser 2400.

Energy dispersive X-ray spectrometric (EDX) measurements were carried out on a Nova NanoSEM230 scanning electron microscope with a tungsten (W) cathode and an EDX unit.

4.3. Synthesis and purification

A typical synthesis involves a solution containing chromium(III) nitrate nonahydrate $Cr(NO_3)_3{\cdot}9H_2O$ (12 g, 30 mmol), acetic acid (X mL, 0–699.4 mmol, X = 0–40) and benzene-1,4-dicarboxylic acid H_2bdc (5 g, 30.1 mmol) in 150-X mL H_2O. The mixture is transferred to the PTFE/Teflon liner in a hydrothermal autoclave which is heated for 20 h at 220 °C and cooled afterwards slowly to room temperature at a rate of 25 °C/h over 8 h.

The contents of the autoclave were transferred to centrifugal tubes and the supernatant solution was carefully removed after centrifugation. Then the resulting solid was stirred in DMF (450 mL) for one hour. The suspension was then again centrifuged. The supernatant liquid phase was discarded and the solid stirred in DMF (450 mL, 16 h). The solid was isolated by centrifugation and the washing step was repeated with ethanol (450 mL for 1 h

and 450 mL or 16 h of stirring). After the final isolation the resulting wet solid was dried in a vacuum oven (120 °C, 12 mbar) for 2 h.

Acknowledgements

The work was supported by the National Natural Science Foundation of China (No. 11372108). L.Y. thanks the Hunan Provincial Innovation Foundation for Postgraduate (CX2017B679). C. J. thanks the BMBF for grant Optimat 03SF0492C.

Appendix A. Supplementary data

Supplementary data associated with this article can be found, in the online version, at https://doi.org/10.1016/j.ica.2017.11.030.

References

[1] G. Férey, Chem. Soc. Rev. 37 (2008) 191–214.
[2] C. Janiak, J.K. Vieth, New. J. Chem. 34 (2010) 2366–2388.
[3] M. Paik Suh, H.J. Park, T.K. Prasad, D.-W. Lim, Chem. Rev. 112 (2012) 782–835.
[4] H. Wu, Q. Gong, D.H. Olson, J. Li, Chem. Rev. 112 (2012) 836–868.
[5] B. Zheng, H. Liu, Z. Wang, X. Yu, P. Yi, J. Bai, CrystEngComm 15 (2013) 3517–3520.
[6] K.A. Cychosz, R. Ahmad, A.J. Matzger, Chem. Sci. 1 (2010) 293–302.
[7] A. Herbst, A. Khutia, C. Janiak, Inorg. Chem. 53 (2014) 7319–7333.
[8] Y. Bai, Y. Dou, L.-H. Xie, W. Rutledge, J.-R. Li, H.-C. Zhou, Chem. Rev. 45 (2016) 2327–2367.
[9] F. Jeremias, D. Fröhlich, C. Janiak, S.K. Henninger, RSC Adv. 4 (2014) 24073–24082.
[10] A. Carné, C. Carbonell, I. Imaz, D. Maspoch, Chem. Soc. Rev. 40 (2011) 291–305.
[11] Y. Zhang, B. Li, H. Ma, L. Zhang, H. Jiang, H. Song, L. Zhang, Y. Luo, J. Mater. Chem. C 4 (2016) 7294–7301.
[12] C. Orellana-Tavra, S.A. Mercado, D. Fairen-Jimenez, Adv. Healthcare Mater. 5 (2016) 2261–2270.
[13] C. Xin, H. Zhan, X. Huang, H. Li, N. Zhao, F. Xiao, W. Wei, Y. Sun, RSC Adv. 5 (2015) 27901–27911.
[14] J. Sánchez-Laínez, B. Zornoza, Á. Mayoral, Á. Berenguer-Murcia, D. Cazorla-Amorós, C. Télleza, J. Coronas, J. Mater. Chem. A 3 (2015) 6549–6556.
[15] G. Férey, C. Mellot-Draznieks, C. Serre, F. Millange, J. Dutour, S. Surble, I. Margiolaki, Science 309 (2005) 2040–2042.
[16] I.M.P. Silva, M.A. Carvalho, C.S. Oliveira, D.M. Profirio, R.B. Ferreira, P.P. Corbi, A.L.B. Formiga, Inorg. Chem. Commun. 70 (2016) 47–50.
[17] A. Buragohain, S. Couck, P. Van Der Voort, J.F.M. Denayer, S. Biswas, J. Solid State Chem. 238 (2016) 195–202.
[18] H.B. Tanh Jeazet, C. Staudt, C. Janiak, Chem. Commun. 48 (2012) 2140–2142.
[19] M. Wickenheisser, C. Janiak, Micropor. Mesopor. Mater. 204 (2015) 242–250.
[20] P. Zhao, N. Cao, W. Luo, G. Cheng, J. Mater. Chem. A 3 (2015) 12468–12475.
[21] D. Jiang, A.D. Burrows, K.J. Edler, CrystEngComm 13 (2011) 6916–6919.
[22] N.A. Khan, I.J. Kang, H.Y. Seok, S.H. Jhung, Chem. Eng. J. 166 (2011) 1152–1157.
[23] S.H. Jhung, J.-H. Lee, J.W. Yoon, C. Serre, G. Férey, J.-S. Chang, Adv. Mater. 19 (2007) 121–124.
[24] J. Ren, N.M. Musyoka, H.W. Langmi, T. Segakweng, B.C. North, M. Mathe, X. Kang, Int. J. Hydrogen Energy 39 (2014) 12018–12023.
[25] S. Wuttke, S. Braig, T. Preiß, A. Zimpel, J. Sicklinger, C. Bellomo, J.O. Rädler, A.M. Vollmar, T. Bein, Chem. Commun. 51 (2015) 15752–15755.
[26] O. de la Iglesia, S. Sorribas, E. Almendro, B. Zornoza, C. Tellez, J. Coronas, Renewable Energy 88 (2016) 12–19.
[27] Y.K. Hwang, D.-Y. Hong, J.-S. Chang, S.H. Jhung, Y.-K. Seo, J. Kim, A. Vimont, M. Daturi, C. Serre, G. Férey, Angew. Chem. Int. Ed. 47 (2008) 4144–4148.
[28] T. Zhao, F. Jeremias, I. Boldog, B. Nguyen, S.K. Henninger, C. Janiak, Dalton Trans. 44 (2015) 16791–16801.
[29] A. Buragohain, S. Couck, P.V.D. Voort, J.F.M. Denayer, S. Biswas, J. Solid State Chem. 238 (2016) 195–202.
[30] K. Leng, Y. Sun, X. Li, S. Sun, W. Xu, Cryst. Growth Des. 16 (2016) 1168–1171.
[31] P.Á. Szilágyi, E. Callini, A. Anastasopol, C. Kwakernaak, S. Sachdeva, R. van de Krol, H. Geerlings, A. Borgschulte, A. Züttelc, B. Damb, Phys. Chem. Chem. Phys. 16 (2014) 5803–5809.
[32] N. Cao, J. Su, W. Luo, G. Cheng, Int. J. Hydrogen Energy 39 (2014) 9726–9734.
[33] X. Zhou, W. Huang, J. Shi, Z. Zhao, Q. Xia, Y. Li, H. Wang, Z. Li, J. Mater. Chem. A 2 (2014) 4722–4730.
[34] J. Pires, M.L. Pinto, C.M. Granadeiro, A.D.S. Barbosa, L. Cunha-Silva, S.S. Balula, V.K. Saini, Adsorption 20 (2014) 533–543.
[35] L.H. Wee, F. Bonino, C. Lamberti, S. Bordigab, J.A. Martensa, Green Chem. 16 (2014) 1351–1357.
[36] W. Salomon, F.-J. Yazigi, C. Roch-Marchal, P. Mialane, P. Horcajada, C. Serre, M. Haouas, F. Taulelle, A. Dolbecq, Dalton Trans. 43 (2014) 12698–12705.
[37] B. Liu, Y. Peng, Q. Chen, Energy Fuels 30 (2016) 5593–5600.
[38] B.S.R. Phani, C.R. Manoj, S. Senthilkumar, S.S. Rajesh, C.B. Hari, Environ. Prog. Sustain. 35 (2016) 461–468.
[39] J. Ren, X. Dyosiba, N.M. Musyoka, H.W. Langmi, B.C. North, M. Mathe, M.S. Onyango, Int. J. Hydrogen Energy 40 (2016) 18141–18146.
[40] Q. Wang, S. Wang, H. Yu, Chin. J. Chem. Eng. 10 (2016) 1481–1486.
[41] T. Wang, P. Zhao, N. Lu, H. Chen, C. Zhang, X. Hou, Chem. Eng. J. 295 (2016) 403–413.
[42] S. Kayal, B. Sun, A. Chakraborty, Energy 91 (2015) 772–781.
[43] J.-Y. Zhang, N. Zhang, L. Zhang, Y. Fang, W. Deng, M. Yu, Z. Wang, L. Li, X. Liu, J. Li, Sci. Rep. 5 (2015) 13514.
[44] Y. Pan, B. Yuan, Y. Li, D. He, Chem. Commun. 46 (2010) 2280–2282.
[45] M. Wickenheisser, A. Herbst, R. Tannert, B. Milow, C. Janiak, Micropor. Mesopor. Mater. 215 (2015) 143–153.
[46] M. Thommes, K. Kaneko, A.V. Neimark, J.P. Olivier, F. Rodriguez-Reinoso, J. Rouquerol, K.S.W. Sing, Pure Appl. Chem. 87 (2015) 1051–1069.
[47] K.S.W. Sing, D.H. Everett, R.A.W. Haul, L. Moscou, R.A. Pierotti, J. Rouquero, T. Siemieniewska, Pure Appl. Chem. 57 (1985) 603–619.
[48] X.X. Huang, L.G. Qiu, W. Zhang, Y.P. Yuan, X. Jiang, A.J. Xie, Y.H. Shen, J.F. Zhu, CrystEngComm 14 (2012) 1613–1617.
[49] F. Yin, G. Li, H. Wang, Catal. Commun. 54 (2014) 17–21.
[50] S. Diring, S. Furukawa, Y. Takashima, T. Tsuruoka, S. Kitagawa, Chem. Mater. 22 (2010) 4531–4538.
[51] S. Hermes, T. Witte, T. Hikov, D. Zacher, S. Bahnmüller, G. Langstein, K. Huber, R.A. Fischer, J. Am. Chem. Soc. 129 (2007) 5324–5325.